Chemical Engineering Science 285 (2024) 119571

Contents lists available at ScienceDirect

Chemical Engineering Science

journal homepage: www.elsevier.com/locate/ces

Machine learning approach for classification of REE/Fe-zeolite catalysts for fenton-like reaction

Óscar Barros [a,b,*], Pier Parpot [a,b], Elisabetta Rombi [c], Teresa Tavares [a,d], Isabel C. Neves [a,b]

[a] CEB - Centre of Biological Engineering, University of Minho, Campus de Gualtar, 4710-057 Braga, Portugal
[b] CQUM, Centre of Chemistry, Chemistry Department, University of Minho, Campus de Gualtar, 4710-057 Braga, Portugal
[c] Dipartimento di Scienze Chimiche e Geologiche, University of Cagliari, Complesso Universitario di Monserrato, 09042 Monserrato, Italy
[d] LABBELS – Associate Laboratory, Braga, Guimarães, Portugal

ARTICLE INFO

Keywords:
Rare earth elements
Zeolite
Fenton-like reaction
Degradation
Machine Learning

ABSTRACT

Various heterogeneous catalysts based on rare earth elements (REE) and iron supported on zeolites were selected and analyzed using machine learning approaches. REE were used in the preparation of multiple REE/Fe-zeolite catalysts with lanthanum, praseodymium or cerium obtained by ion exchange or impregnation methods, using FAU or MFI structures as supports. The efficiency of these REE/Fe-zeolite catalysts was examined in Fenton-like reaction, in the degradation of tartrazine (Tar) and indigo carmine (IC) as selected organic pollutants in the aqueous solution. The REE/Fe-zeolite catalysts demonstrated outstanding performance, with Tar being degraded by over 80% and IC 95%. Machine learning algorithms were employed for clustering and classification of the different catalysts, based on their performance. Unsupervised learning algorithms like Principal Component Analysis and K-Means were used for pattern recognition while supervised classifiers were employed to classify the heterogeneous catalysts, considering their ability to degrade dyes by Fenton reaction.

1. Introduction

Rare earth elements (REE) are widely used due to their diversified properties such as optical, electrical, metallurgical, catalytic and magnetic (An et al., 2013; Çelik et al., 2015; Negrea et al., 2018; Unal Yesiller et al., 2013), allowing different daily applications (Balaram, 2019; Rostami et al., 2019; Zhao et al., 2016). Due to the extensive demand and price, their reutilization is important, but the recycling technology is still in the early stages (Barros et al., 2019; Gutiérrez-Gutiérrez et al., 2015; Lyman, and Palmer, 1993; Otto and Wojtalewicz-Kasprzak, 2014; Yang et al., 2013). The hardship in REE recycling is mainly due to the complexity of the process and to the very different amounts of those elements in the end products, ranging from mg to kg (Binnemans et al., 2013).

The application of REE in catalysis is gaining attention, as there is a strong interest in designing and developing new heterogeneous catalysts, especially sustainable and cost-effective ones (Zheng et al., 2022). The definition of a heterogeneous catalyst loaded with recovered REE can be a key-factor for redox reactions applied in environment rehabilitation. Furthermore, these new catalysts can be applied in advanced oxidation processes (AOP) for wastewater treatment (Giannakis et al., 2015; Miklos et al., 2018; Sievers, 2011; Zheng et al., 2022). Zeolites, which have been reported as suitable supports (Assila et al., 2023; Barros et al., 2019; Mosai et al., 2019; Mosai and Tutu, 2021), are inorganic crystalline microporous aluminosilicates (Li and Yu, 2021; Sable et al., 2021; Xu et al., 2007). They have been used in many catalytic reactions for the production of high-value chemicals (Xu et al., 2007), including Fenton reactions (Gonzalez-Olmos et al., 2012; Sable et al., 2021). The Fenton reaction is a process that utilizes hydrogen peroxide (H_2O_2) and iron to degrade organic pollutants and is widely used for environmental remediation (Jain et al., 2018). During the typical reaction, hydroxyl radicals ($^{\bullet}OH$) can be generated in the presence of H_2O_2 and Fe^{2+} (Imlay, 2006; Pignatello et al., 2006), which are highly reactive and can effectively break down organic molecules (Buxton et al., 1988) into non-toxic products such as CO_2, H_2O and inorganic salts (Dong et al., 2018).

Dyes are widely used in various industries such as food, pharmaceutical and cosmetic ones, to provide color and visual appeal to products. However, in recent years, their use has raised concerns about their potential health and environmental impacts. Two dyes that have received significant attention are tartrazine (E102) and indigo carmine (E132). Tartrazine (E102) is a synthetic yellow food dye widely used in

* Corresponding author.
E-mail address: oscar.barros@ceb.uminho.pt (Ó. Barros).

https://doi.org/10.1016/j.ces.2023.119571
Received 15 August 2023; Received in revised form 13 November 2023; Accepted 27 November 2023
Available online 29 November 2023

various food and beverage products (Assila et al., 2023; Silva et al., 2022) that is linked to some adverse health effects (Neelam and Mishra, 2018), such as allergic reactions, hyperactivity in children and migraines. Indigo carmine (E132) is a blue dye that colors different food and drinks (Silva et al., 2022). It has been linked to multiple adverse effects, such as allergic reactions, nausea and skin rashes (Neelam and Mishra, 2018). These dyes were proved to be degraded by heterogeneous Fenton-type reaction in the presence of H_2O_2 and Fe^{3+} (Assila et al., 2023).

Machine Learning (ML) approach is useful for selecting the best catalyst among a significant number of prepared REE-zeolite catalysts that were evaluated by the degradation of dyes in aqueous medium through Fenton-type reaction. ML is a branch of artificial intelligence that involves the development of algorithms and statistical models for pattern recognition, predictions or decisions without being explicitly programmed (Jordan and Mitchell, 2015). The capacity of ML algorithms to evaluate large amounts of data from catalytic reactions and catalyst characterization can help to design the best catalyst according to its performance for a given reaction (Kitchin, 2018; Li et al., 2018). Several applications of both homogeneous and heterogeneous catalysis have been using ML (Yang et al., 2020).

The aim of this work is to evaluate the usage of zeolites loaded with REE recovered from contaminated wastewater to act as efficient heterogeneous catalysts for Fenton-type reaction. The prepared REE/Fe-zeolite catalysts will be tested in the degradation of tartrazine and indigo carmine. Different ML algorithms will be used to select the best catalyst, also highlighting the importance of the ML approach in the determination of the effect of chemical properties of the catalyst on its performance.

2. Materials and methods

2.1. Materials

REE used in this research were cerium ($Ce(NO_3)_3{\cdot}6H_2O$; 99.5 %; Acros Organics), lanthanum, ($La(NO_3)_3{\cdot}6H_2O$; 99.9 %; Alfa Aesar) and praseodymium ($PrCl_3{\cdot}xH_2O$; 99.9 %; Alfa Aesar). These metals were used from previously prepared stock solutions at 1 g/L. The multi-element ICP quality control standard solution, with a concentration of each element under study of 200 mg/L, was purchased from CPAchem. The solution from iron(III) nitrate ($Fe(NO_3)_3{\cdot}9H_2O$, Aldrich) was prepared as required. A stock solution of 90 mM of hydrogen peroxide (H_2O_2, 30 wt%, Merck) was prepared.

For this work, two zeolite structures were used: (NH_4)ZSM5 from MFI (CBV3024E, Si/Al = 15.00) and NaY (CBV100, Si/Al = 2.80) in powder form obtained from Zeolyst International and NaX in powder or pellets, Sigma-Aldrich (Si/Al = 1.64 and Si/Al = 1.50, respectively), both from FAU.

The tartrazine dye (Tar, $C_{16}H_9N_4Na_3O_9S_2$, ≥ 90 %) was purchased from Sigma Aldrich, while the indigo carmine (IC, $C_{16}H_8N_2Na_2O_8S_2$, ≥ 90 %) was obtained from Merck. Deionized water for dye solutions was produced with an ultrapure water system (Milli-Q, EQ 7000).

2.2. REE/Fe-zeolite catalysts preparation

The REE/Fe-zeolite catalysts were prepared by ion exchange or by impregnation methods in liquid phase. In the first method, a solution of the individual REE (La, Ce or Pr) of 10 or 25 mg/L with and without a controlled pH (4.00) was added to a suspension containing 16 g/L of zeolite, with an orbital shake of 120 rpm for 24 h. After the REE doping, the REE-zeolite was dried and added to the Fe^{3+} solution (10 mg/L) till a final concentration of 6 g/L was reached, with and without a controlled pH (4.00) and with an orbital shake at 120 rpm for 24 h. Finally, the suspension was filtered off, washed with deionized water, dried at 60 °C overnight and calcined at 350 °C for 4 h under a dry–air stream. For impregnation, the addition of the REE or Fe follows the same conditions used in ion-exchange method, with the only exception being the lack of a filtration. The resulting solution was decanted, leaving the catalysts to be dried and then calcinated in the same conditions. The prepared heterogeneous catalysts are displayed in Table 1.

2.3. Catalysts characterization

Attenuated Total Reflectance Fourier Transform Infrared spectroscopy (ATR-FTIR) analysis was performed at room temperature using a PerkinElmer Spectrum Two spectrometer equipped with an ATR accessory. A diamond prism was used as the waveguide. All spectra were recorded with a resolution of 2 cm^{-1} in the wavelength region 4000–400 cm^{-1} by averaging 50 scans.

Elemental quantification of the La, Ce, Pr and Fe in the solutions used for metal addition to the zeolites was performed using an ICP-OES spectrometer (Optima 8000, PerkinElmer). The REE quantification is similar to the one described by *Barros et al.* (Barros et al., 2019) with slightly different operating conditions: RF power at 1400 W, argon plasma flow at 12 L/min, auxiliary gas flow at 0.2 L/min and nebulizer gas flow at 0.70 L/min. The wavelength (nm) used were: Fe – 238.204, La – 408.672, Ce – 413.764 and Pr – 390.844, with radial plasma view for Fe and axial view for the REE.

The chemical analysis of the catalyst was performed to quantify La, Ce, Pr, Fe, Si, Al and Na in the solid samples (0.05 g). These were submitted to microwave assisted acid digestion and the resulting solution was analyzed with a 5110 ICP-OES spectrometer (Agilent Technologies). The protocol used to process these samples is similar to that described by *Assila et al.* (Assila et al., 2023).

2.4. Fenton-like reaction

Catalytic runs were carried out in a semi-batch reactor at atmospheric pressure and 40 °C, under continuous stirring (300 rpm), using a solution of 30 mg/L of tartrazine or indigo carmine, at a specific concentration of hydrogen peroxide (H_2O_2). The initial concentration of dyes (30 ppm), pH (3.00) and temperature (40 °C) were fixed at optimal values determined in a preliminary evaluation of the degradation of organic pollutants using similar zeolite-based LaFe catalysts (Assila et al., 2023). The runs were divided into initial screening (IS) and catalytic tests (CT). Once the assay started, samples were taken at fixed time intervals and the reaction was stopped with the addition of an excess of $NaHSO_3$, which instantaneously consumes the unreacted H_2O_2.

In order to select the best catalyst, an initial screening (IS) was carried out with sampling at the beginning of the run and after 180 min, using a catalyst concentration of 0.8 g/L with 0.5 mL of H_2O_2 at a specific concentration. The remaining conditions of the assay are equal to

Table 1
Designation and details of REE/Fe-zeolite catalysts and respective method of preparation.

Samples	Label	Zeolite type	pH	Method
$La_{10}Fe_{10}NaX$	A3	FAU powder	4.00	impregnation
$La_{10}Fe_{10}NaX$	A7	FAU pellet	4.00	impregnation
$La_{10}Fe_{10}ZSM5$	Z1	MFI	4.00	impregnation
$La_{10}Fe_{10}NaY$	Z2	FAU	4.00	impregnation
$La_{25}Fe_{10}ZSM5$	Z3	MFI	4.00	impregnation
$La_{25}Fe_{10}NaY$	Z4	FAU	4.00	impregnation
$La_{10}Fe_{10}ZSM5$	Z15	MFI	4.00	ion exchange
$La_{25}Fe_{10}ZSM5$	Z16	MFI	4.00	ion exchange
$La_{25}Fe_{10}NaY$	Z17	FAU	without	ion exchange
$Ce_{10}Fe_{10}ZSM5$	Z5	MFI	4.00	ion exchange
$Ce_{10}Fe_{10}NaY$	Z6	FAU	4.00	ion exchange
$Ce_{25}Fe_{10}ZSM5$	Z7	MFI	4.00	ion exchange
$Ce_{25}Fe_{10}NaY$	Z8	FAU	4.00	ion exchange
$Pr_{10}Fe_{10}ZSM5$	Z9	MFI	4.00	ion exchange
$Pr_{10}Fe_{10}NaY$	Z10	FAU	4.00	ion exchange
$Pr_{25}Fe_{10}ZSM5$	Z11	MFI	4.00	ion exchange
$Pr_{25}Fe_{10}NaY$	Z12	FAU	4.00	ion exchange

the ones described above. The catalytic tests (CT) were carried out with REE/Fe-zeolite catalysts with liquid samples taken at fixed intervals of time during 300 min, using a catalyst concentration of 0.8 g/L. The effects of the H_2O_2 load were assessed by using 5.0 or 0.5 mL at a specific concentration.

In all tests, the samples taken were centrifuged at 12000 rpm for 10 min and the liquid was analyzed. The dye concentrations measurements by UV–vis spectroscopy were performed with a microplate spectrophotometer Epoch 2 from Biotek using the characteristic wavelengths λ_{max} = 427 nm and 610 nm for Tar and IC, respectively.

Usual Fenton-like reactions are described by a pseudo first-order kinetic model (Gonzalez-Olmos et al., 2012) that is used to evaluate the parameters of the degradation of the dyes and its non-linear equation is described by Eq. (1):

$$\frac{C_t}{C_0} = e^{-k^*\left(\frac{W}{V}\right)^*t} \tag{1}$$

C_t (mg/L) is the concentration of dye at a given time t; C_0 (mg/L) is the initial concentration of dye; k (L/(g*min)) is the rate constant; V (L) is the volume of the solution; W (g) is the mass of catalyst used for the assay and t (min) is the time. A linear form could be achieved according to the following Eq. (4):

$$\ln\left(\frac{C_t}{C_0}\right) = -m^*t \tag{2}$$

2.5. Machine learning analysis

ML analysis was conducted using a table designed as DataFrame, with the different catalysts produced as rows, while the different columns or features were filled with the REE and Fe concentrations obtained by the catalyst chemical analysis, the ratio between these two concentrations and the Si/Al ratio. Adding to that information, the dyes degradation reached in the IS and CT assays was also considered as feature.

Supervised and unsupervised ML approaches were applied to all catalytic results. For the unsupervised learner, the Principal Component Analysis, PCA, (method for reducing the dimensionality of data, leading to an increased interpretation and minimizing information loss) and K-Means clustering (division of the samples into groups or clusters that are more compatible with each other accordantly to the studied conditions) were used. For these analyses, a scaling or normalization of the data is required before using PCA and K-Means.

The supervised learner uses classification to divide the tested catalysts into good or bad ones, accordantly to their results. K-nearest neighbors' classifier (KNN), Decision Tree Classifier, Random Forest and Logistic Regressor Classifier were used to classify the samples. These classifiers are often used in binary classification. In this study, a binary classification approach was employed to evaluate the performance of each catalyst with respect to the degradation of the dye. Based on the obtained degradation results, each dye was classified according to the percentage of conversion. Next, a mean value taking into account the results obtained for different catalysts and experimental conditions, allows the preliminary selection of the best catalyst. This approach enables the efficiently evaluation and comparison of the performances of the catalysts in a standardized manner (Table 2).

Table 2
Binary classification used for each REE/Fe-catalyst.

Degradation intervals	Degradation Classification	Classification means	Binary Classification
80 < Deg < 100	1	Mean value >	1
60 < Deg < 80	2	4.75	
40 < Deg < 60	3		
20 < Deg < 40	4	Mean value ≤	0
0 < Deg < 20	5	4.75	

To develop and evaluate the model's performance, the dataset was divided into two sets: a training set (70 % of the data), which contains known output and enables the model to learn how to generalize and apply to new data, and a test set (30 % of the data), which was used to evaluate the model's prediction accuracy. The data was divided using a stratified approach, ensuring that both the training and test sets had the same proportion of each class.

All tests were performed using Spyder (Python 3.9) and the required modules for the python analysis as pandas, numpy, scikit-learn, matplotlib and seaborn.

2.6. Statistical analysis

The initial screening (IS) results were statistically analyzed using One-Way ANOVA, through which all samples were compared between themselves. The catalytic tests (CT) results were analyzed using Two-Way ANOVA. Bonferroni's multiple comparison test was used for the different comparisons performed. The tests were performed using the software Graph Pad Prism version 8.0.2 (Graph Pad Software, Inc, San Diego, CA, USA). The results were considered significantly different only when the probability (p-value) was lower than 0.05, assuming a 95 % confidence interval.

3. Results and discussion

The catalysts prepared by the entrapment of REE and Fe in zeolite supports were used on the degradation of two different organic pollutants in water. Tartrazine is a mono-azo molecule and Indigo Carmine (IC) is an indigoid molecule, both soluble in water, being easily oxidized by Fenton reaction. Both organic molecules are almost flat with molecular dimensions of 16.94 Å x 4.41 Å for Tar, and 17.98 Å x 7.41 Å for IC, taking in account the maximum ellipsoid axes (Figure S1). FAU zeolite (NaY and NaX) has an average aperture of pores of 7.4 Å, while MFI (ZSM5) is a medium pore size zeolite with pore diameters of 5.4 to 5.6 Å. Although the size of the molecules to de degraded is bigger than the average pore diameter, the pore size distribution is quite spread in the case of ZSM5 making a relevant part of the porosity available for the retention of each of the substrates. In fact, these zeolite structures present different values in their textural properties, specifically the surface area due to mesoporosity (S_{meso}) (Assila et al., 2023; Barros et al., 2019), Table S1. ZSM5 has a S_{meso} of 185 m2/g, while FAU has a S_{meso} of 19 and 67 m2/g for NaY and NaX, respectively. The existence of this mesopore surface area is reflected in the Vmeso, providing dyes with an increased surface for adsorption and subsequent catalysis. In order to select the best FAU catalyst and to compare with the MFI-based ones, Tar degradation was carried out with the catalysts prepared with La and Fe. In a previous work (Barros et al., 2019), NaX was used to remove REE from aqueous solutions and it was found that this zeolite was an effective adsorbent (Barros et al., 2019). For this reason, NaX, prepared by impregnation in the same experimental conditions used for the other REE/Fe-zeolite catalysts, is also included for evaluation as a heterogeneous catalyst (in pellet or powder) for the Fenton-like reaction (Fig. 1).

The best results were obtained with the catalysts based on MFI structure (Z15 and Z1), followed by NaY (Z2) and NaX (A3 and A7), as shown in Table S2. The significant differences calculated by the column analysis performed using One-Way ANOVA are shown in Table S3. The last one, the powder form (A3) favors the Fenton-like reaction in comparison with the pellets (A7), as mass transfer limitations are reduced as the average size of the catalysts particles diminishes. The lower degradation efficiency obtained for NaX was expected since this type of zeolite is mainly used for adsorption processes (Barros et al., 2019) rather than for catalysis.

Moreover, Z2 ($La_{10}Fe_{10}NaY$) reached higher conversion than any of the NaX catalysts, as NaY zeolite is widely used in catalytic applications (Kuźniarska-Biernacka et al., 2013; Santos et al., 2020; Shannon, 1976),

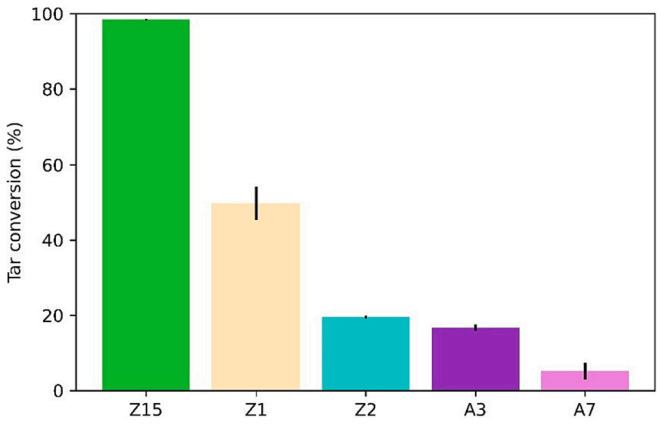

Fig. 1. Tar degradation in the presence of MFI: $La_{10}Fe_{10}$ZSM5 (Z15) prepared by ion exchange ( ) and $La_{10}Fe_{10}$ZSM5 (Z1) by impregnation ( ); FAU: $La_{10}Fe_{10}$NaY (Z2) prepared by impregnation ( ); $La_{10}Fe_{10}$NaX (A3, powder,) and $La_{10}Fe_{10}$NaX (A7, pellet,) prepared by impregnation. Conditions of the reaction: 20 mg of catalyst/25 mL of a 30 ppm solution of Tar; 0.5 mL of H_2O_2 90 mM; pH = 3; T = 40 °C; t = 180 min.

as it enhances the catalytic role of the supported metal. In addition, Z15 ($La_{10}Fe_{10}$ZSM5), prepared by the ion exchange method, reached higher degradation efficiency than Z1 ($La_{10}Fe_{10}$ZSM5), prepared by the impregnation method, due to fact that the metallic active species are better distributed on the internal surface area (Kuźniarska-Biernacka et al., 2011; Santos et al., 2020). Since NaY and ZSM5 loaded with catalytic metals act as bifunctional catalysts, enhancing the metal role within the desired reaction, they are expected to have advantage over NaX as supports for heterogeneous catalysis.

These last REE/Fe-zeolite catalysts were analyzed by FTIR (Fig. 2).

The characteristic bands of the pristine zeolite structures (FAU and MFI) dominate the spectra of all REE/Fe-zeolite catalysts. The band characteristic of the δ(H_2O) vibration mode of absorbed water on zeolite was identified at 1640 cm^{-1}, whereas the typical bands of the lattice vibrations of the framework are evidenced in the range 1330–450 cm^{-1} (Assila et al., 2023; Costa et al., 2004; Villalba et al., 2010). The band at 960 cm^{-1} is attributed to the asymmetric stretching of Si–O and Al–O bonds belonging to SiO_4 and AlO_4 tetrahedra (Boroglu and Gurkaynak, 2011; Wang et al., 2015), whereas the bands at 670 cm^{-1} and near 750 cm^{-1} are related to the Si–O symmetric stretching and oscillations of aluminosilicate oxygen tetrahedral chains (Boroglu and Gurkaynak, 2011; Wang et al., 2015). The band at about 550 cm^{-1} is attributed to the symmetric stretching vibrations of bridge bonds, Si–O–Si and bending vibrations of O–Si–O (Aronne et al., 2002).

The particle size of the NaX pristine structures may have an impact over the spectra of A3 (powder) and A7 (pellets) while the catalysts preparation method seems not to influence the spectra of the two ZSM5-based catalysts (Z1 and Z15).

In addition, the framework Si/Al ratio of the samples based on FAU structure can be determined by FTIR analysis using the following Eq. (3) (Aronne et al., 2002):

$$x = 3.857\text{-}0.00621W_{DR} \quad (3)$$

where $x = (1 + Si/Al)^{-1}$ and W_{DR} is the wavenumber at 500–650 cm^{-1}, related to the vibrations of the FAU lattice (Aronne et al., 2002) (Table 3).

The framework Si/Al values of FAU-based catalysts show that Z2 and A3 were the most affected by the introduction of both metals, La and Fe. The reduction of the Si/Al ratio for A3 may be related with the acid character of the metals solution. The powder form of A3, with larger surface area, makes it more sensitive to its circumstances than A7 with a pelleted form and smaller surface area. The lower degradation performance of A3 and Z2 is probably related to the impregnation method used in their preparation, which affects more the zeolite structure than the ion exchange method. The impregnation method results in a weak metal-support interaction and large metal sites are obtained, while ion exchange reaches a finer metal dispersion (Kuźniarska-Biernacka et al., 2011), with reactional advantages. The larger metal sites resulting from the impregnation method led to a reduced conversion efficiency.

Based on the obtained catalytic results, ZSM5 and NaY structures were selected as the supports to prepare the REE/Fe-zeolite catalysts for degrading Tar and IC through the Fenton-like reaction. These selected structures exhibit excellent thermal and chemical stability and possess the ability to retain multiple metal ions through ion-exchange reaction, thereby offsetting the framework negative charge. The pristine zeolites NaY and ZSM5 exhibit distinct average particle sizes. NaY displays uniform particles ranging from 100 to 750 nm in size, while ZSM5 show

Table 3
Framework Si/Al ratios obtained from the FTIR analysis.

Label	Samples	Framework Si/Al
–	NaY	2.80
–	NaX	1.64
A3	$La_{10}Fe_{10}$NaX	1.44
A7	$La_{10}Fe_{10}$NaX	1.64
Z2	$La_{10}Fe_{10}$NaY	2.49

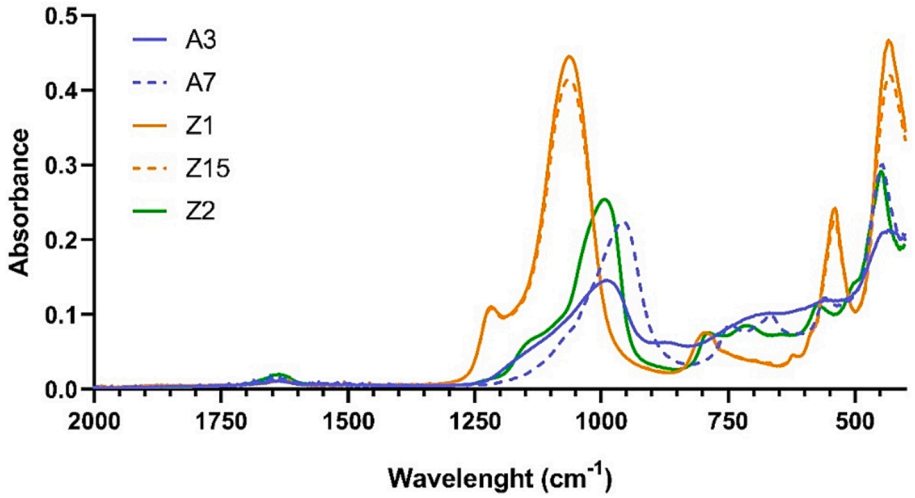

Fig. 2. FTIR spectra of the REE/Fe-zeolite catalysts in the spectral region of 2000 to 450 cm^{-1}.

heterogeneous particles, including large aggregates, medium-sized particles (measuring 2500 and 760 nm) and small particles (>100 nm) (Peixoto et al., 2021).

Tar degradation was carried out in the same reaction conditions as those in Fig. 1 (Assila et al., 2023). IC degradation was instead performed using two different H_2O_2 concentrations, 90 and 12 mM. It was proven (data not shown) that a 7.5 fold increase in H_2O_2 concentration is not justified, as it does not lead to any improvement in degradation performance after 180 min of reaction.

Previous evaluations (Assila et al., 2023) demonstrated that there is almost no adsorption of the dye on the catalysts, its removal is mainly due to the catalytic degradation by Fenton-like reaction.

3.1. Selection of the best REE/Fe-zeolite catalyst using IS results

The results for the PCA analysis are shown in Fig. S2A, after the scaling of the DataFrame. Two principal components, PCA 1 and PCA 2 (variables created from the linear composites of the original variables with the highest variance), were selected to build the PCA, and the same value was obtained with the Knee Locator method (Satopaa et al., 2011). The results obtained for PCA are shown in Fig. 3A. These results show a biplot where the bottom *x* and left *y* are used for samples distribution, while the top *x* and right *y* are used for the distribution of the different features.

The cos of the angle between the features analyzed indicates their correlation. Values close to 1 (angle near 0°) indicate that features are directly correlated, values near −1 (angle near 180°) indicate indirect correlation and values next to 0 (angle near 90°) show no correlation. The CT for Tar and IC, the IS for Tar and IS, the Si/Al ratio and the Fe/REE ratio seem to have some direct correlation between each other. This positive correlation suggests that the ratios Si/Al and Fe/REE might have an influence on the degradation of the tested dyes, foreseeing that the catalysts with higher ratios have better catalytic properties. It is reported in different applications that catalysts with higher Si/Al ratio have a higher activity and higher selectivity (Li et al., 2023). Apparently, there is no correlation with the preparation methods or with the Fe concentration. Adding to that, a negative correlation between degradation and REE concentration in the zeolites was found, suggesting that increasing concentrations of REE seem not to improve dyes degradation. A higher amount of REE on the catalysts surface might not imply a better dye degradation, just larger active sites not as efficient as smaller but more dispersed ones. Fe concentration have a positive correlation with the impregnation preparation method and a negative correlation with the ion exchange, indicating that the catalysts produced by impregnation reach a higher Fe concentration than the ones made via ion exchange.

The catalysts group division based on the results of the PCA could be performed in diverse ways and for that reason it was tested by K-Means algorithm, shown in Fig. 3B. This analysis provided four clusters based on the Elbow method, presented in Fig. S2B and confirmed by the Knee Locator method. Group (1) consists in Z5, Z7, Z9, Z11, Z15 and Z16, group (2) in Z2, Z4 and Z17, group (3) in Z1 and Z3 and finally, group 4 in Z6, Z8, Z10 and Z12. The groups (1) and (3) seem to be more influenced by the values of Si/Al and Fe/REE ratios as well as by the results of the degradations tests for both dyes. This suggests that these groups may include the best catalysts (possibly Z15, Z16 and Z3), mainly due to the stronger influence of the degradation results of Tar and IC.

Group (2) appears to be primarily affected by the concentration of La and by the impregnation method, whereas group (3) key determinants were the concentrations of Pr and Ce, along with the ion exchange method. Important to mention that group (1) includes catalysts designed with all REE of interest, while group (3) and group (2) include only La catalysts and group 4 includes only Ce and Pr catalysts.

The combination shown in Fig. 3 helps to perform a division between groups considering the zeolite type and the preparation method. For example, the zeolite type division would consist of groups (1) and (3), both related to the higher Si/Al ratio, which is characteristic of the ZSM5 zeolite used as support for these catalysts, while groups 2 and 4 should have a lower Si/Al, characteristic of NaY zeolite. The preparation method division would consist in groups (2) and (3), as both used the impregnation method, while groups 1 and 4 used the ion exchange protocol. It is important to mention that the preparation method division just includes the results for La catalysts, as this was the only REE involved in both methods. Therefore, these observations will help to assess the extent of the possible differences between the catalysts accordantly to the previously mention characteristics.

The dye degradation obtained with the catalysts based on the two zeolite types and the REE concentration on the starting solution are highlighted in Fig. 4. The best catalytic results for the degradation of both dyes by Fenton-like reaction were obtained for ZSM5 as support (Fig. 4) and validated by statistical differences presented in Table S4. These results are related to the physiochemical properties of the ZSM5 which enhance a better dispersion of the metals.

Remarkably, in the case of IC dye degradation, the performance of the catalysts is similar between La, Ce or Pr for the same support. The worst results considering these three metals were obtained with the NaY supported catalysts, with a slight IC dye degradation enhanced in the presence of Ce or Pr (Table S4). Overall, these results confirm the observations described in Fig. 3A, making possible to visualize a remarkable difference in the degradation of the dyes when considering the zeolites used as supports of the catalysts. This was shown in Fig. 3A, where catalysts with higher Si/Al ratio will also promote a higher conversion of the dyes in the IS and CT assays.

Only one significant difference was found between Z1 and Z16 (based on ZSM5 with different preparation methods) for Tar degradation in what concerns the effect of the REE concentration, as shown in Table S5. The only difference suggests an improvement of the catalyst when using higher REE concentration in the preparation solution by ion exchange. For IC, the catalytic results may be divided into two groups. The first one includes the catalysts with Ce and with Pr. Only one significant difference was found between Z6 and Z8 (ZSM5) for the IC degradation with the increment of the REE concentration in starting solution from 10 to 25 mg/L, as shown in Table S5.

The second group includes the catalysts produced using La. Significant differences were found between Z1 and Z3 (based on ZSM5 by impregnation with 10 and 25 mg/L La, respectively); Z1 and Z16 (based on ZSM5 and prepared by the two methods, with 10 and 25 mg/L La, respectively), and Z2 and Z17 (based on NaY with different preparation methods, different pH approaches and with 10 and 25 mg/L La in the starting solution, respectively), in the IC degradation. In the first two cases, higher concentration of REE implies an improvement in the dye degradation. The same conclusion is not validated by the comparison between Z2 and Z17 as too many parameters are affecting simultaneously the degradation mechanism.

It is possible to evaluate the differences between the tested REE, Fig. 4. For the same metal concentration in the starting solution and the same support, it can be seen that the conversions obtained with La catalyst were the best for Tar. Five significant differences were found for Tar conversion (four for ZSM5 and one for NaY), as shown by Table S6. The significant differences between the La catalysts Z15 and Z16 versus Ce or Pr supported on ZSM5, imply that the La catalysts reach higher conversions during the IS assays than the other REE. The Z17 and Z8 NaY catalysts achieved low conversions, but with significant differences, which could indicate an influence of the REE in the catalyst performance. The preparation method, impregnation versus ion exchange, could also justify some differences, but this hypothesis was not supported as there was no significant difference between Z17 and Z12, NaY catalysts with Pr.

Regarding the IC conversion, nine significant differences were found (two for ZSM5 and seven for NaY), as shown by Table S6. The differences between the samples of La/Fe-ZSM5, Z1, confirm that this catalyst is not good for IC degradation as shown in Fig. 4. The detected differences are

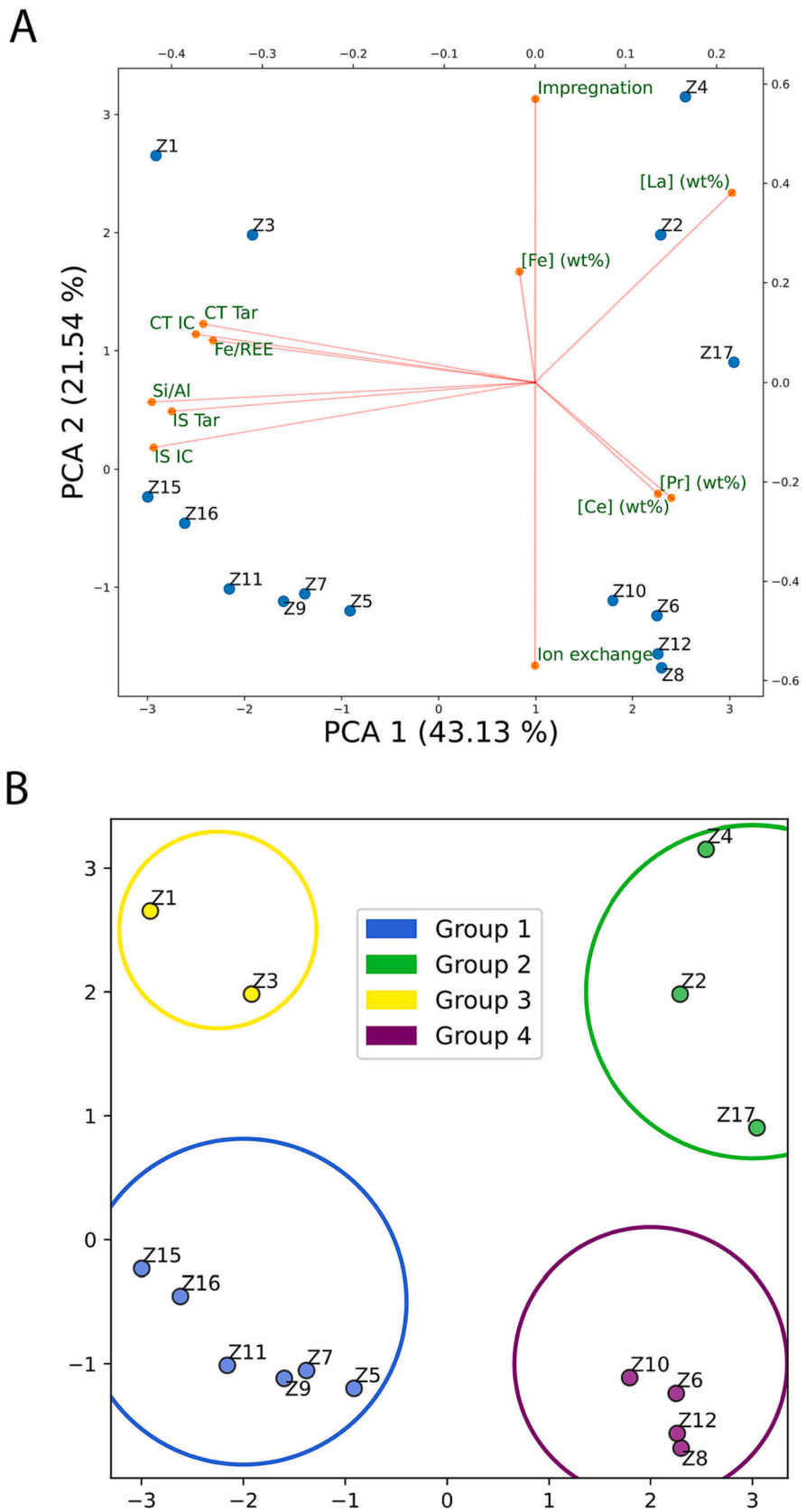

Fig. 3. Graphical distribution of the ML analysis for the different catalysts: **A**) PCA analysis; **B**) K-Means algorithm. The IS and CT values are referred to initial screening and catalytically tests, respectively, for Tar and for IC.

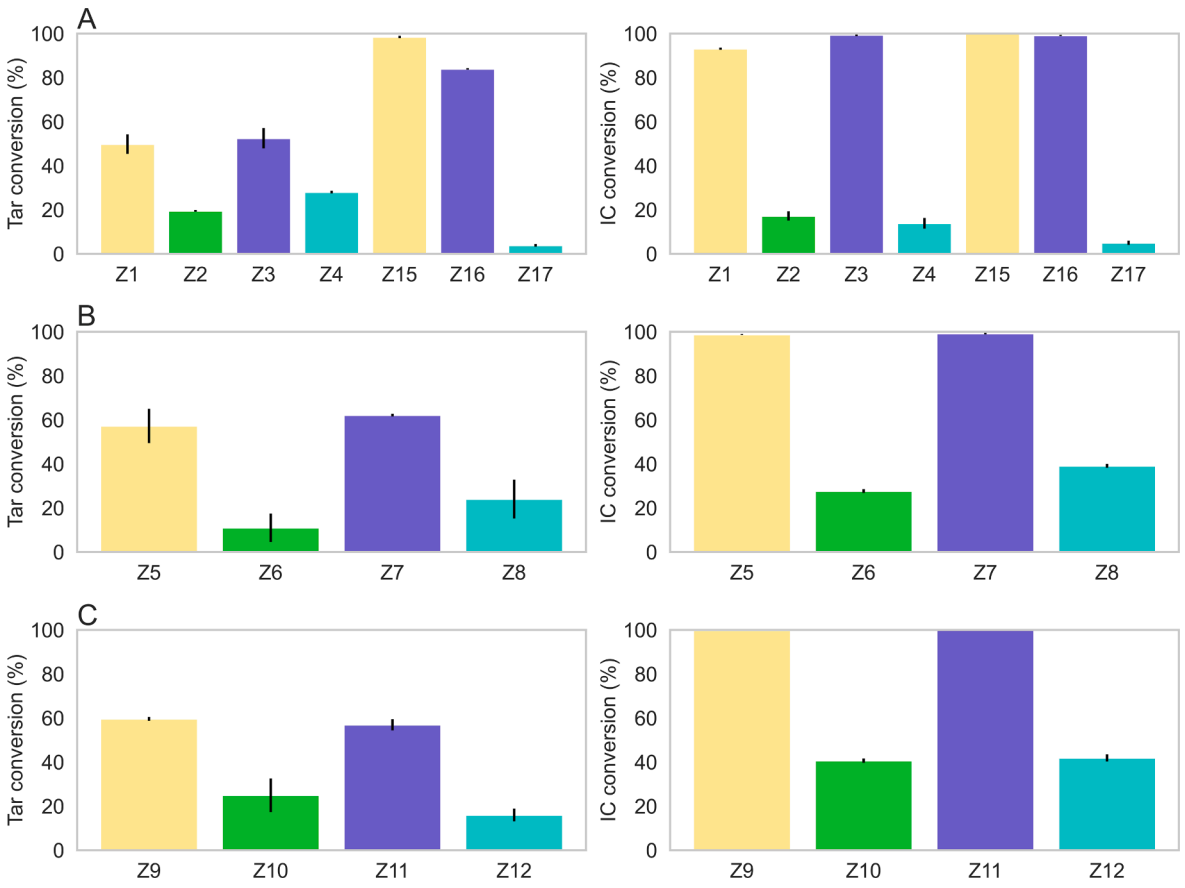

Fig. 4. Degradation of Tar and IC using the REE/Fe-zeolite catalysts for **A**) La, **B**) Ce and **C**) Pr, after IS test. The catalysts are divided into ZSM5 (MFI) with a REE concentration of 10 mg/L ( ) and 25 mg/L ( ); NaY (FAU) with a REE concentration of 10 mg/L ( ) and 25 mg/L ( ). Conditions of the reaction: 20 mg of catalyst/25 mL at 30 ppm of dye; 0.5 mL of 90 mM of H_2O_2 for Tar and of 12 mM of H_2O_2 for IC; pH = 3; T = 40 ^{0}C and 3 h of reaction.

related not only with the REE but also with the catalysts preparation method. On the other hand, Pr/Fe-NaY catalyst reached better conversion than with La or with Ce. In this case, these differences are more related with the REE rather than with the preparation method.

The last division shown in the PCA distribution, Fig. 3A, regards the catalysts preparation method. The evaluation of the importance of this parameter only includes La/Fe-zeolite catalysts, the only ones prepared by the two methods, impregnation and ion exchange. NaY supported catalysts reached low degradations, but they will be kept in this analysis to assess the influence of the preparation method. The results are shown in Fig. 5.

The catalytic performance of Z3 ($La_{25}Fe_{10}$ZSM5 by impregnation), Z15 ($La_{10}Fe_{10}$ZSM5 by ion exchange) and Z16 ($La_{25}Fe_{10}$ZSM5 by ion exchange) are very similar. The Z1 ($La_{10}Fe_{10}$ZSM5 by impregnation)

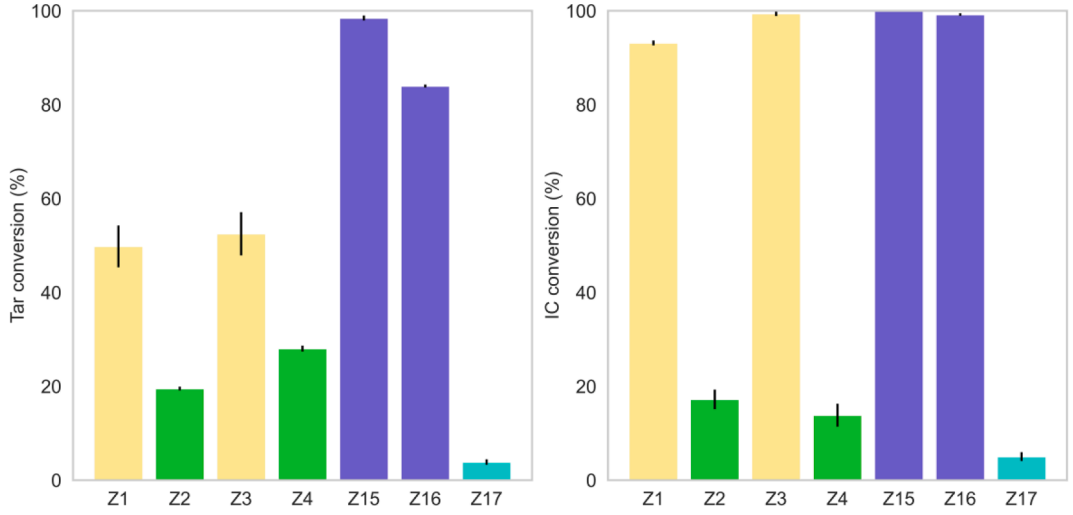

Fig. 5. IS conversion of the two dyes by La/Fe catalysts prepared by different methods. The catalysts are divided into ZSM5 (MFI) with impregnation ( ) and ion exchange ( ); NaY (FAU) with impregnation ( ) and ion exchange ( ). Conditions of the reaction: 20 mg of catalyst/25 mL at 30 ppm of dye; 0.5 mL of 90 mM H_2O_2 for Tar and 12 mM H_2O_2 for IC; pH = 3; T = 40 °C and 3 h of reaction.

have significant differences compared to those catalysts for the IC degradation, as shown in Tables S5 and S7. For Tar degradation, those differences are more visible, with the best catalytic results being obtained with the La/Fe-ZSM5 prepared by the ion-exchange method, Z15 and Z16 (Table S7).

The NaY catalysts Z2 and Z4 provide better conversions with a significant difference when compared with Z17 (Table S7), which suggest that in this case, the impregnation method enhances the pollutant degradation, probably due to more metallic sites on the surface of the catalyst, leading to an increase of •OH. However, the results obtained with the La/Fe-NaY catalysts are worse than the ones obtained with ZMS5 as support, as stated before.

The dye degradation results attained with La/Fe-ZSM5 suggest that the ion exchange method for the preparation the catalysts is better than the impregnation method. The degradation dissimilarities are related to the different amounts of the metals added to the zeolites depending on the preparation method. A chemical analysis by ICP-AES of the digested REE/Fe-zeolites was performed (Table 4).

Both zeolite structures are more selective for iron than for REE. NaY reaches higher metal loading than ZSM5 due to their lower Si/Al ratio, 2.80 compared to 15.00 for ZSM5, which results in a higher ion exchange capacity of the FAU structure. In addition, the amounts of La and of Ce in NaY are similar, with a ratio Fe/REE ranging from 1.67 to 1.55 for La and between 2.50 and 1.33 for Ce, depending on the concentrations of the initial solutions. The same effect is not observed for Pr on NaY, in which the ratio Fe/REE is higher than for the others REE, with 5.8 to 2.8 for a REE concentration of 0.11 and 0.21 wt%, respectively. Independently of the REE used on the FAU structure, a decrease in the total Si/Al ratio was registered in the samples prepared at pH 4.00 by impregnation (Z2 or Z4) or by ion-exchange (Z6, Z8, Z10 and Z12) when compared to the respective pristine zeolite. The sample Z17 prepared by ion-exchange shows a decrease in the Si/Al ratio compared to the pristine NaY (Si/Al = 2.80), which confirms that the acidic media affect the FAU structure by dealumination, especially the Fe solution with a pH of 3.37, while the pH of the La solution was 5.91.

The introduction of REE or Fe only slightly affects the MFI structure, especially in the case of Ce (Z5 and Z7) or Pr (Z9 and Z11), since the total Si/Al ratio of these samples are very close to the pristine zeolite, 15.00. The Si/Al ratio is more affected when the catalysts are prepared by impregnation (Z1 and Z3). With the increase in La concentration in sample Z3, the ratio of Fe/REE significantly decreases. A similar but not so severe effect was observed for the other REE, Pr (Z10 and Z12).

The REE adsorption on MFI structures, after 24 h assays, ranged between 23 and 35 % for La, 47 and 68 % for Ce, 24 and 38 % for Pr, of the original amount of the sorbates in solution. FAU structures are even more efficient in adsorbing REE and Fe than MFI due to their higher ion-exchange capacity. The difference in the ionic radius of sorbates: Fe^{3+} (0.63 Å), La^{3+} (1.03 Å), Ce^{3+} (1.01 Å) and Pr^{3+} (0.99 Å) justifies the selectivity of both structures for Fe in detriment of REE.

In summary, there is a clear difference between the two zeolite structures and the REE/Fe-ZSM5 catalysts have the best degradation results with both dyes by Fenton-like reaction. Adding to that, there is also a difference between the degradation achieved by the catalyst depending on the REE on its surface, as La catalyst tends to reach better results than the ones containing Ce and Pr. The ion exchange method proved to be the best option for the REE/Fe-catalyst preparation. Finally, an increase in the REE concentration in the initial solution seems not to be relevant, given the similarity of the dye conversions for the same support and same REE, with some exceptions. The lack of significant differences of the pollutant conversion can justify the use of the starting solution with the lowest concentration that allows the degradation reaction.

Combining these informations, it is possible to conclude that within the tested possibilities the best catalysts is the La/Fe-ZSM5 produced via the ion exchange method, with the minimal amount of REE that promotes the dye degradation. The collected data will allow to evaluate the performance of Machine Learning classification algorithms and their ability to correctly identify the best REE/Fe-zeolite catalyst, based on accurate information.

Each sample was considered using a binary classification, where 0 corresponds to a bad performance, while 1 is regarded as a good one. The binomial classification was carried out in agreement with Table 2 and the result was added to the previous data frame. This classification resulted in two REE/Fe-catalysts with a classification of 1, while the rest had a classification of 0. Then, the classification was carried out using KNN, Decisions Trees, Random Forests classifiers and Logistic Regression. The results for the different classifiers are shown in Fig. 6.

The KNN Classifier, Fig. 6A, selected one neighbor (n_neighbors) accordingly to the accuracy values for both training and test sets, as shown in Fig. S2C. The Decision tree (Fig. 6A) used a random state of 20, the Random Forest (Fig. 6B) used 10 for n estimators with the same random state and the Logistic Regression used the same random state (Fig. 6A). For the classifiers, it is crucial to avoid overfitting concerning the training set, as it is for the learning process. A suitable generalization of the model from the training set should be validated by the test set in order to obtain a good classification for new and unseen data. Overall, the classifiers were able to separate the two best catalysts from all the tested ones, by using the data relating each catalyst to its classification.

Initially each classifier was evaluated with the respective *scores* related to the accuracy of the values under consideration (*x* and *y* values of training and test data), as shown in Table 5.

The *scores* obtained for the different classifiers are 100 % except for Random Forest and for Logistic Regression for the training set, which is a good result considering that three over four classifiers presented 100 % of accuracy in the test set and two over four reached 100 % for the training set. An evaluation was performed using the classification report, which gives a summary of percentages values of precision, recall and f1-scores (Table 6). The precision is related to the accuracy of making good predictions, the recall is the value of the correctly identified positive predictions and the f1-score is the harmonic mean of the precision and recall. Another vital metric to assess the classification used is the confusion matrix. For this evaluation, the real classification from the binary classification (*y_real*) and the predicted classification (*y_pred*) calculated from the model were used.

All classifiers, with the exception of Random Forest, presented a 100 % score for the precision, recall and f1-scores of the prediction advanced by the model. All classifiers tested are very similar, except for Random Forests, and the overall result is shown in Figure S3. For the best models there were only true positives (the model predicted it was true, and it was actually true) and true negatives (the model predicted it was false and it was actually false) values identified.

This evaluation verified that two of the 15 REE/Fe-zeolite catalysts were selected as the best ones, namely Z15 ($La_{10}Fe_{10}$ZSM5) and Z16 ($La_{25}Fe_{10}$ZSM5). These catalysts were prepared with ZSM5, as Fig. 4

Table 4
Chemical analysis of the solid REE/Fe-zeolite catalysts.

Sample	Label	Si/Al	REE (wt%)	Fe (wt%)	Fe/REE
$La_{10}Fe_{10}$ZSM5	Z1	13.72	0.02	0.88	40.0
$La_{10}Fe_{10}$NaY	Z2	2.31	0.18	0.30	1.67
$La_{25}Fe_{10}$ZSM5	Z3	14.70	0.06	0.48	7.33
$La_{25}Fe_{10}$NaY	Z4	2.30	0.47	0.73	1.55
$La_{10}Fe_{10}$ZSM5	Z15	14.57	0.04	0.85	20.5
$La_{25}Fe_{10}$ZSM5	Z16	14.59	0.04	0.66	16.0
$La_{25}Fe_{10}$NaY	Z17	2.50	0.52	0.84	1.63
$Ce_{10}Fe_{10}$ZSM5	Z5	15.06	0.02	0.43	20.0
$Ce_{10}Fe_{10}$NaY	Z6	2.40	0.17	0.42	2.50
$Ce_{25}Fe_{10}$ZSM5	Z7	14.90	0.04	0.46	10.5
$Ce_{25}Fe_{10}$NaY	Z8	2.37	0.42	0.56	1.35
$Pr_{10}Fe_{10}$ZSM5	Z9	15.02	0.02	0.39	17.0
$Pr_{10}Fe_{10}$NaY	Z10	2.38	0.11	0.63	5.80
$Pr_{25}Fe_{10}$ZSM5	Z11	14.89	0.02	0.30	14.0
$Pr_{25}Fe_{10}$NaY	Z12	2.35	0.21	0.59	2.8

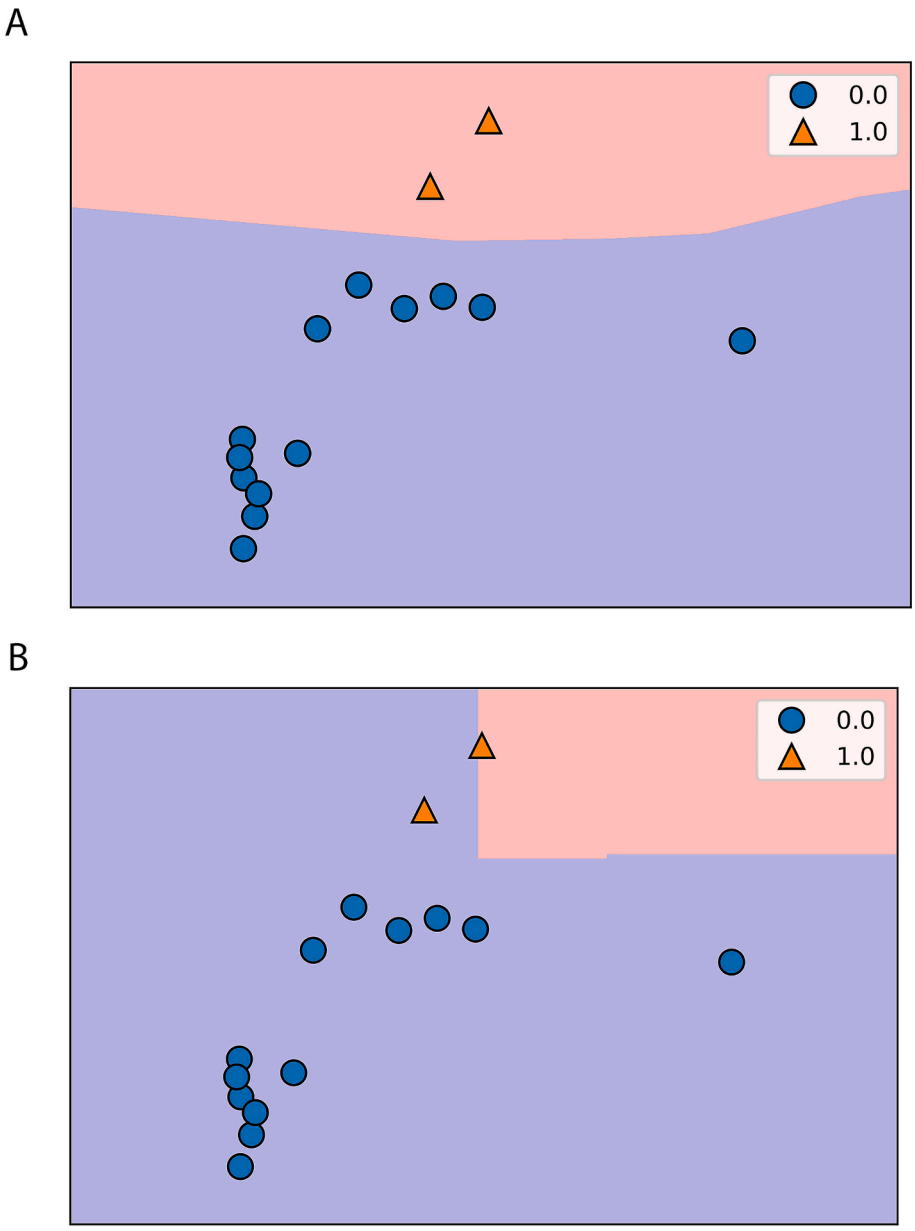

Fig. 6. Classification of all different REE/Fe-zeolite catalysts using ML algorithms: **A**) KNN classifier, Decision Tree classifier and Logistic Regression and **B**) Random Forest classifier. The 1 represent a good catalyst, while the 0 is a bad catalyst accordantly to the evaluation performed.

Table 5
Scores obtained for the different classification algorithms.

Classifier	KNN	Decision Tree	Random Forest	Logistic Regression
Training score	100 %	100 %	80 %	90 %
Test score	100 %	100 %	90 %	100 %

indicates that this zeolite is the best support and shows that La is the best REE of the three tested for the catalytic reaction. From Fig. 4, 10 and 25 mg/L were the initial solution concentrations selected for that support, confirming that there is no difference between the two in terms of pollutants degradation. Finally, these catalysts were prepared by the ion exchange method, as it was the best method for ZSM5, as shown in Fig. 5.

The Pearson correlation was calculated to evaluate the relation of the different features used and to see how they correlate with each other,

Table 6
Classification of catalysts by classifier algorithms for the test set. The results include precision, recall and f1-score.

Classifier		KNN		Decision Tree		Random Forest		Logistic Regression	
Catalyst classification		*Bad*	*Good*	*Bad*	*Good*	*Bad*	*Good*	*Bad*	*Good*
Model Performance	*Precision*	100	100	100	100	80	0	100	100
	recall	100	100	100	100	100	0	100	100
	f1-score	100	100	100	100	89	0	100	100

and the results are displayed as a heatmap, Fig. 7.

The results of Fig. 7 display three important relations, one of them being that the correlation between the IS and CT results of both dyes is greater than 0.70. This suggests that a good catalyst would have good conversions in the tested assays. The Si/Al ratio and Fe/REE ratio have a high positive correlation (between 0.7 and 0.9) (Mukaka, 2012), suggesting that catalysts with higher Si/Al ratio, namely the ZSM5, will tend to prefer Fe over REE. The same high positive correlation is found between the Si/Al have and the overall results for IS and CT, supporting that the ZSM5 zeolite was the best support to prepare the catalysts. The Fe/REE ratio seemed to have moderate positive correlation (between 0.5 and 0.7) (Mukaka, 2012) with the results from IS and from CT, suggesting that it could be expected a better conversion of the tested dyes with higher values of Fe/REE ratio.

The Fe/REE ratio have a low negative correlation (between − 0.3 and − 0.5) (Mukaka, 2012) with the REE concentrations used as predictable, since the higher REE concentrations the smaller Fe/REE. In opposition, the Fe/REE have a low positive correlation (between 0.3 and 0.5) (Mukaka, 2012) with the Fe concentration. The CT and IS correlation with the La concentration is low negative, but with Ce and with Pr is negligible (between – 0.3 to 0.0) (Mukaka, 2012). It was expected a more positive correlation between the CT and IS results and the La concentration as the best conversions were obtained with this REE. There is a very high negative correlation (-0.9 to −1.0) (Mukaka, 2012) between the impregnation method and the ion exchange method. This is predictable since the catalysts were made using one of the two procedures. Finally, the vast majority of the other correlations are negligible, as the values range between 0 and 0.3 or between 0 and −0.3 (Mukaka, 2012).

The ML algorithms are an important tool that allowed us to determine the main influences on each produced catalyst performance using 12 features. It was possible to develop a classification model that successfully predicted the classes of unseen data and was an important asset in selecting the best catalyst. Finally, it is possible to improve these models by increasing the number of characteristic features, a larger data collection (in this case, more catalysts) and by testing different algorithms parameters. These changes can lead to an improved model, which can provide a better understanding of the processes under consideration and the selection of the best solutions for the purpose. On the other hand, improving the data frames with more features could lead to the successful application of regression models, which could help to predict the degradation of untested catalysts or even other characteristics.

Z15 ($La_{10}Fe_{10}$ZSM5) and Z16 ($La_{25}Fe_{10}$ZSM5) catalysts were used in kinetic studies, assessing the effect of La concentration on the catalyst performance over time.

3.2. Catalytic tests (CT)

The catalytic tests with 0.8 g/L of REE/Fe catalysts (Z15 and Z16) for 300 min of reaction were carried out in two parts. First, the effect of the hydrogen peroxide concentration in the reaction was evaluated by the addition of two different volumes of H_2O_2 (0.5 and 5 mL) at specified concentrations, 90 mM and 12 mM. In a second part, a kinetic model for dyes degradation by Fenton-like reaction was established for the best REE/Fe-ZSM5 catalysts.

The dyes were degraded using the selected catalysts in the presence

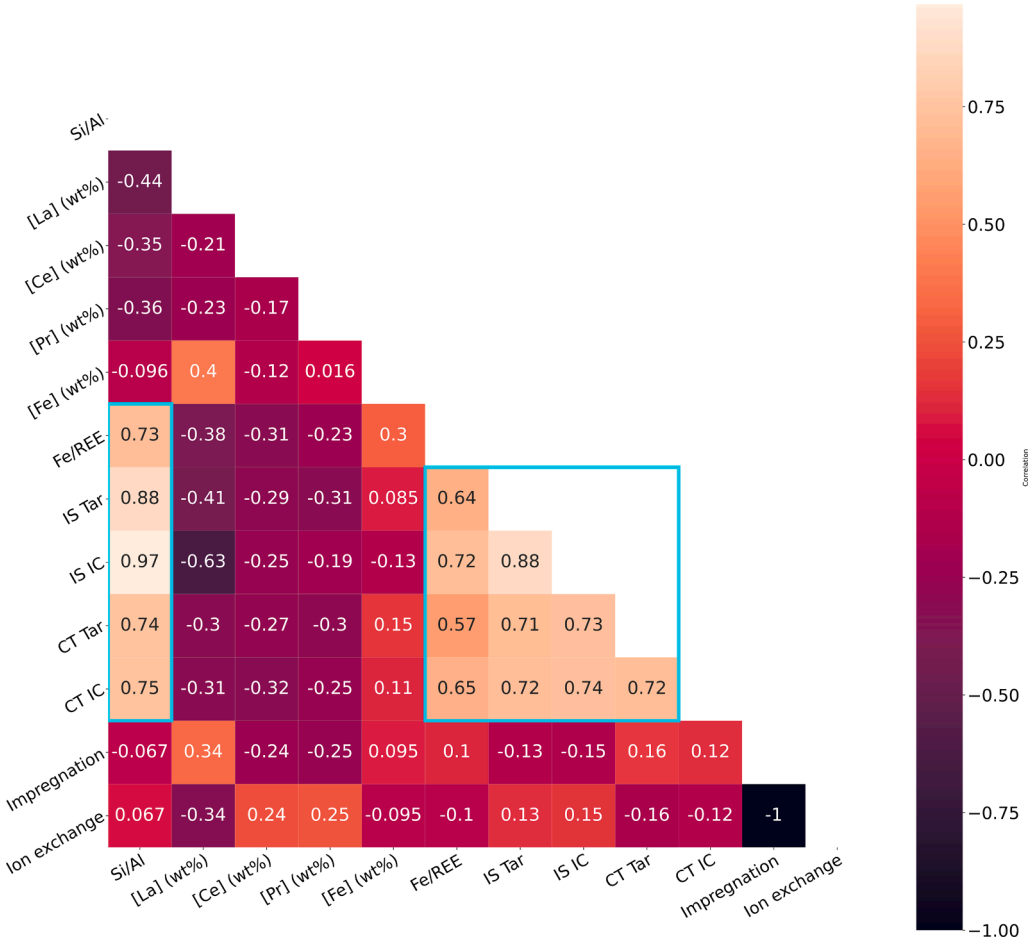

Fig. 7. Heatmap representing the Pearson correlation between the different features considered on the degradation assays. The left scale represents the different correlation values and the respective colors.

of H_2O_2 (Fig. 8). As expected, higher concentration of H_2O_2 enhances the degradation of the dyes (Table S8). The best reactional conditions were established (Table S9). Z15 ($La_{10}Fe_{10}$ZSM5) and Z16 ($La_{25}Fe_{10}$ZSM5) catalysts differ in the La concentration used in the preparation solution and, therefore, in the available La ions in the zeolite for exchanging (Table 4). In fact, both samples have similar catalytic performance as shown in Table S9. Probably this is related to the small amount of La (0.04 wt%) present in both catalysts, despite Z15 has more iron (0.85 wt %) than Z16 (0.66 wt%).

As the select REE/Fe-ZSM5 catalysts and H_2O_2 have an important role in the degradation of the dyes by Fenton-like reaction, it would be interesting to examine the reaction rate. For that, the fitting parameters of the pseudo-first order model were obtained taking in account 50 % of the dyes degradation using the two selected catalysts. The non-linear and linear equations were used to fit the data with reduced errors. The results are shown in Table 7. The respective graphical representation of the kinetic modelling is shown in Figure S4.

Considering the R^2, Sy.x and the SSR results, the non-linear form of the pseudo-first order model seems to fit better the experimental data than the linear form.

The highest values of the rate constant, *k*, are observed for Z16 catalyst for both dyes. The main difference between Z15 and Z16 for the IC degradation is that the Z16 catalyst required 30 min less to achieve a degradation near 50 % than Z15 (Fig. 8). In the Z16, the compromise between the amount of REE (0.04 w%) and Fe (0.66 wt%) seems to be the best to achieve a fast degradation in the first minutes of reaction. The high kinetic constant is related to the presence of the La^{3+} and Fe^{3+} in the zeolite, which favors the formation of $HO^{\bullet}$ radicals responsible for dyes degradation.

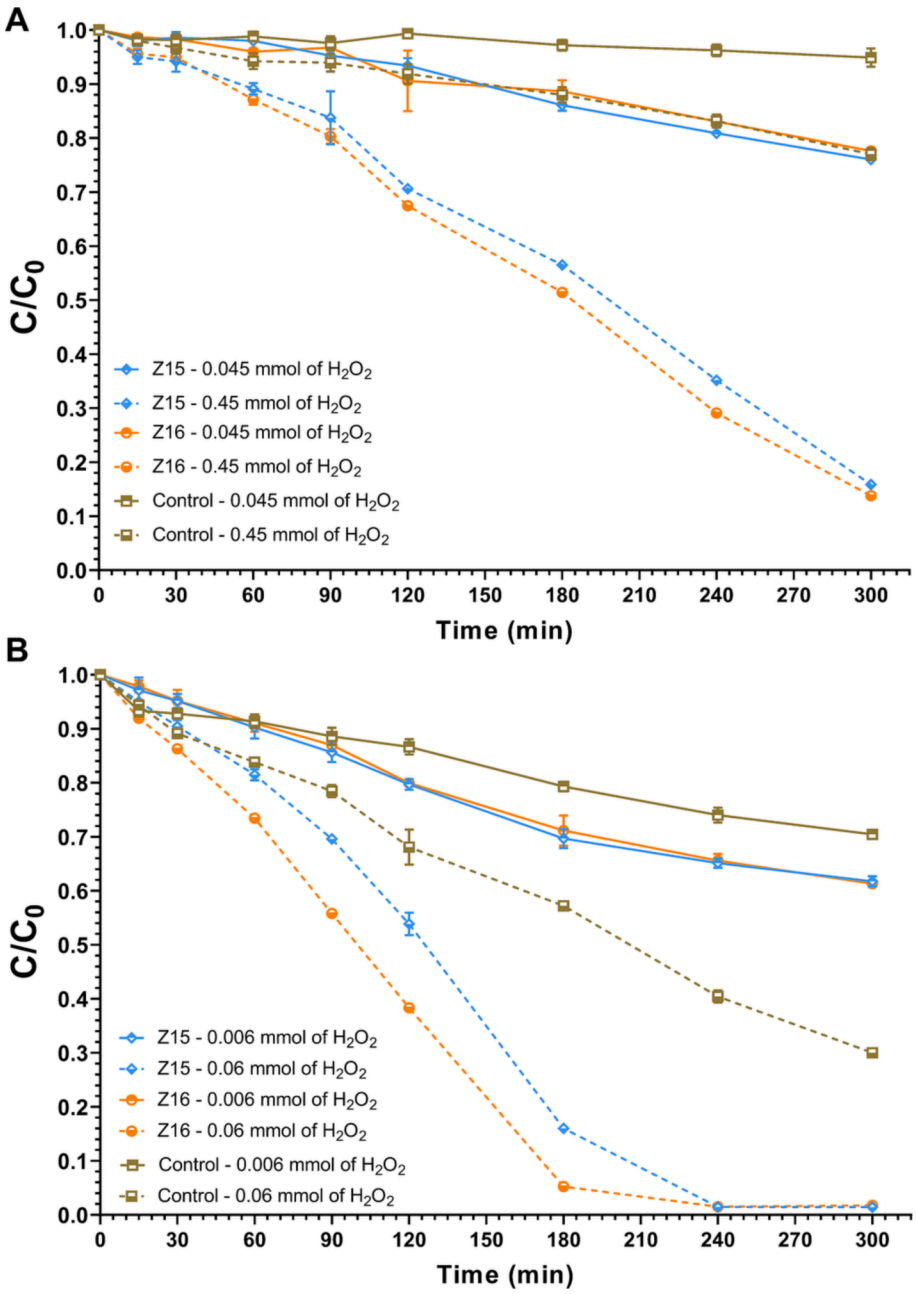

Fig. 8. Conversion by Fenton-like reaction over time of Tar (**A**) and of IC (**B**) using the selected catalysts (Z15 and Z16) and the controls. The degradation assisted with 0.5 mL of H_2O_2 is represented with a full line, while the reaction with 5 mL of H_2O_2 used a dashed line. Conditions of reaction: 200 mg of catalyst/250 mL at 30 ppm of dye; 0.5 mL or 5 mL of 90 mM H_2O_2 for Tar and 12 mM H_2O_2 for IC; pH = 3; T = 40 ^{0}C and 300 min of reaction.

Table 7
Kinetic results for the degradation of both dyes using the non-linear (eq. (1) and the linear (eq. 4) forms of the pseudo-first order model equation.

Catalyst		Tar		IC	
		Z15	Z16	Z15	Z16
non-linear	df[a]	25	27	23	19
	K^b	0.0035	0.0039	0.0054	0.0073
	R^2	0.9556	0.9500	0.9550	0.9777
	Sy.x[c]	0.0299	0.0371	0.0344	0.0237
	SSR[d]	0.0224	0.0371	0.0273	0.0107
linear	df[a]	25	27	23	19
	K^b	0.0039	0.0046	0.0039	0.0046
	R^2	0.9651	0.9645	0.9551	0.9776
	Sy.x[c]	0.0351	0.0433	0.0472	0.0332
	SSR[d]	0.0307	0.0505	0.0511	0.0209

[a] degrees of freedom.
[b] K (L/(g*min)).
[c] standard deviation of the residuals.
[d] sum of squares due to regression.

4. Conclusions

Several REE/Fe-zeolite catalysts based on two zeolitic structures, FAU or MFI, were prepared and evaluated on Fenton-like reaction for the degradation of Tar or IC dyes. The selection of the best catalyst taking into account different parameters was achieved by machine learning approaches. La^{3+} together with Fe^{3+} supported on MFI zeolite structure prepared by ion-exchange reached the best catalytic results. Unsupervised ML tools like PCA and K-Means were a crucial help to visualize and to form clusters according to best: zeolite structure, REE used and synthesis method. The classifiers from the ML proved to be helpful in narrowing the number of catalysts from fifteen to only two, for the selection of the best degradation catalyst. The catalyst $La_{10}Fe_{10}$ZSM5, Z15, obtained via ion exchange method, was the best catalyst selected by ML with a significant dyes degradation efficiency by Fenton-like reaction.

CRediT authorship contribution statement

Óscar Barros: Conceptualization, Data curation, Investigation, Software, Formal analysis, Writing – original draft. **Pier Parpot:** Validation, Software, Writing – review & editing. **Elisabetta Rombi:** Validation, Writing – review & editing. **Teresa Tavares:** Conceptualization, Writing – review & editing, Validation, Supervision. **Isabel C. Neves:** Conceptualization, Writing – review & editing, Validation, Supervision.

Declaration of competing interest

The authors declare that they have no known competing financial interests or personal relationships that could have appeared to influence the work reported in this paper.

Data availability

Data will be made available on request.

Acknowledgments

O. Barros thanks FCT for the concession of his Ph.D. grant (SFRH/BD/140362/2018). This study was supported by the Portuguese Foundation for Science and Technology (FCT) under the scope of the strategic funding of UID/BIO/04469/2020 and UID/QUI/0686/2020 units and BioTecNorte operation (NORTE-01-0145-FEDER-000004) funded by the European Regional Development Fund under the scope of Norte2020—Programa Operacional Regional do Norte, Portugal. The authors thank to Dr. Filipe Teixeira from CQUM for determine the size of the molecules by Molden Software.

Appendix A. Supplementary data

Supplementary data to this article can be found online at https://doi.org/10.1016/j.ces.2023.119571.

References

An, F., Gao, B., Huang, X., Zhang, Y., Li, Y., Xu, Y., Zhang, Z., Gao, J., Chen, Z., 2013. Selectively removal of Al(III) from Pr(III) and Nd(III) rare earth solution using surface imprinted polymer. React. Funct. Polym. 73, 60–65. https://doi.org/10.1016/j.reactfunctpolym.2012.08.022.

Aronne, A., Esposito, S., Ferone, C., Pansini, M., Pernice, P., 2002. FTIR study of the thermal transformation of barium-exchanged zeolite A to celsian. J. Mater. Chem. 12, 3039–3045. https://doi.org/10.1039/b203859e.

Assila, O., Barros, Ó., Fonseca, A.M.F., Parpot, P., Soares, O.S.G.P., Pereira, M.F.R., Zerrouq, F., Kherbeche, A., Rombi, E., Tavares, T., Neves, I.C., 2023. Degradation of pollutants in water by Fenton-like oxidation over LaFe-catalysts: optimization by experimental design. Microporous Mesoporous Mater. 349, 112422 https://doi.org/10.1016/j.micromeso.2022.112422.

Balaram, V., 2019. Rare earth elements: a review of applications, occurrence, exploration, analysis, recycling, and environmental impact. Geosci. Front. 10, 1285–1303. https://doi.org/10.1016/j.gsf.2018.12.005.

Barros, Ó., Costa, L., Costa, F., Lago, A., Rocha, V., Vipotnik, Z., Silva, B., Tavares, T., 2019. Recovery of rare earth elements from wastewater towards a circular economy. Molecules 24, 1005. https://doi.org/10.3390/molecules24061005.

Binnemans, K., Jones, P.T., Blanpain, B., Van Gerven, T., Yang, Y., Walton, A., Buchert, M., 2013. Recycling of rare earths: a critical review. J. Clean. Prod. 51, 1–22. https://doi.org/10.1016/j.jclepro.2012.12.037.

Boroglu, M.S., Gurkaynak, M.A., 2011. Fabrication and characterization of silica modified polyimide–zeolite mixed matrix membranes for gas separation properties. Polym. Bull. 66, 463–478. https://doi.org/10.1007/s00289-010-0286-x.

Buxton, G.V., Greenstock, C.L., Helman, W.P., Ross, A.B., 1988. Critical Review of rate constants for reactions of hydrated electrons, hydrogen atoms and hydroxyl radicals (·OH/·O− in Aqueous Solution. J. Phys. Chem. 17, 513–886. https://doi.org/10.1063/1.555805.

Çelik, İ., Kara, D., Karadaş, C., Fisher, A., Hill, S.J., 2015. A novel ligandless-dispersive liquid–liquid microextraction method for matrix elimination and the preconcentration of rare earth elements from natural waters. Talanta 134, 476–481. https://doi.org/10.1016/j.talanta.2014.11.063.

Costa, F., Silva, C.J.R., Raposo, M.M.M., Fonseca, A.M., Neves, I.C., Carvalho, A.P., Pires, J., 2004. Synthesis and immobilization of molybdenum complexes in a pillared layered clay. Microporous Mesoporous Mater. 72, 111–118. https://doi.org/10.1016/j.micromeso.2004.04.003.

Dong, C., Ji, J., Shen, B., Xing, M., Zhang, J., 2018. Enhancement of H2O2 decomposition by the co-catalytic effect of WS 2 on the Fenton reaction for the synchronous reduction of Cr(VI) and remediation of phenol. Environ. Sci. Technol. 52, 11297–11308. https://doi.org/10.1021/acs.est.8b02403.

Giannakis, S., Gamarra Vives, F.A., Grandjean, D., Magnet, A., De Alencastro, L.F., Pulgarin, C., 2015. Effect of advanced oxidation processes on the micropollutants and the effluent organic matter contained in municipal wastewater previously treated by three different secondary methods. Water Res. 84, 295–306. https://doi.org/10.1016/j.watres.2015.07.030.

Gonzalez-Olmos, R., Martin, M.J., Georgi, A., Kopinke, F.-D., Oller, I., Malato, S., 2012. Fe-zeolites as heterogeneous catalysts in solar Fenton-like reactions at neutral pH. Appl. Catal. B Environ. 125, 51–58. https://doi.org/10.1016/j.apcatb.2012.05.022.

Gutiérrez-Gutiérrez, S.C., Coulon, F., Jiang, Y., Wagland, S., 2015. Rare earth elements and critical metal content of extracted landfilled material and potential recovery opportunities. Waste Manag. 42, 128–136. https://doi.org/10.1016/j.wasman.2015.04.024.

Imlay, J.A., 2006. Iron-sulphur clusters and the problem with oxygen. Mol. Microbiol. 59, 1073–1082. https://doi.org/10.1111/j.1365-2958.2006.05028.x.

Jain, B., Singh, A.K., Kim, H., Lichtfouse, E., Sharma, V.K., 2018. Treatment of organic pollutants by homogeneous and heterogeneous Fenton reaction processes. Environ. Chem. Lett. 16, 947–967. https://doi.org/10.1007/s10311-018-0738-3.

Jordan, M.I., Mitchell, T.M., 2015. Machine learning: Trends, perspectives, and prospects. Science (80-) 349, 255–260. https://doi.org/10.1126/science.aaa8415.

Kitchin, J.R., 2018. Machine learning in catalysis. Nat. Catal. 1, 230–232. https://doi.org/10.1038/s41929-018-0056-y.

Kuźniarska-Biernacka, I., Biernacki, K., Magalhães, A.L., Fonseca, A.M., Neves, I.C., 2011. Catalytic behavior of 1-(2-pyridylazo)-2-naphthol transition metal complexes encapsulated in Y zeolite. J. Catal. 278, 102–110. https://doi.org/10.1016/j.jcat.2010.11.022.

Kuźniarska-Biernacka, I., Carvalho, M.A., Rasmussen, S.B., Bañares, M.A., Biernacki, K., Magalhães, A.L., Rolo, A.G., Fonseca, A.M., Neves, I.C., 2013. Copper(II)–imidasalen complexes encapsulated into NaY zeolite for oxidations reactions. Eur. J. Inorg. Chem. 2013, 5408–5417. https://doi.org/10.1002/ejic.201300656.

Li, J., Gao, M., Yan, W., Yu, J., 2023. Regulation of the Si/Al ratios and Al distributions of zeolites and their impact on properties. Chem. Sci. 14, 1935–1959. https://doi.org/10.1039/D2SC06010H.

Li, Z., Wang, S., Xin, H., 2018. Toward artificial intelligence in catalysis. Nat. Catal. 1, 641–642. https://doi.org/10.1038/s41929-018-0150-1.
Li, Y., Yu, J., 2021. Emerging applications of zeolites in catalysis, separation and host–guest assembly. Nat. Rev. Mater. 6, 1156–1174. https://doi.org/10.1038/s41578-021-00347-3.
Lyman, J.W., Palmer, G.R., 1993. Recycling of rare earths and iron from NdFeB magnet scrap. High Temp. Mater. Process. 11, 175–188. https://doi.org/10.1515/HTMP.1993.11.1-4.175.
Miklos, D.B., Remy, C., Jekel, M., Linden, K.G., Drewes, J.E., Hübner, U., 2018. Evaluation of advanced oxidation processes for water and wastewater treatment – a critical review. Water Res. 139, 118–131. https://doi.org/10.1016/j.watres.2018.03.042.
Mosai, A.K., Chimuka, L., Cukrowska, E.M., Kotzé, I.A., Tutu, H., 2019. The recovery of rare earth elements (REEs) from aqueous solutions using natural zeolite and bentonite. Water, Air, Soil Pollut. 230, 188. https://doi.org/10.1007/s11270-019-4236-4.
Mosai, A.K., Tutu, H., 2021. Simultaneous sorption of rare earth elements (including scandium and yttrium) from aqueous solutions using zeolite clinoptilolite: a column and speciation study. Miner. Eng. 161, 106740 https://doi.org/10.1016/j.mineng.2020.106740.
Mukaka, M.M., 2012. Statistics corner: A guide to appropriate use of correlation coefficient in medical research. Malawi Med. J. 24, 69–71.
Neelam, M., Mishra, S., 2018. Effects of food additives and preservatives on processed food. Asian J. Sci. Appl. Technol. 7, 30–32. https://doi.org/10.51983/ajsat-2018.7.2.1031.
Negrea, A., Gabor, A., Davidescu, C.M., Ciopec, M., Negrea, P., Duteanu, N., Barbulescu, A., 2018. Rare earth elements removal from water using natural polymers. Sci. Rep. 8, 316. https://doi.org/10.1038/s41598-017-18623-0.
Otto, R., Wojtalewicz-Kasprzak, A., 2014. Patent. Method for Recovery of Rare Earths from Fluorescent Lamps. USOO8628734B2.
Pignatello, J.J., Oliveros, E., MacKay, A., 2006. Advanced oxidation processes for organic contaminant destruction based on the fenton reaction and related chemistry. Crit. Rev. Environ. Sci. Technol. 36, 1–84. https://doi.org/10.1080/10643380500326564.
Rostami, I., Rezvani, H., Hu, Z., Shahmoradian, S.H., 2019. Breakthroughs in medicine and bioimaging with up-conversion nanoparticles. Int. J. Nanomedicine 14, 7759–7780. https://doi.org/10.2147/IJN.S221433.
Sable, S.S., Georgi, A., Contreras, S., Medina, F., 2021. Fenton-like oxidation of phenol with in-situ generated hydrogen peroxide and Pd/Fe-zeolite catalysts. Water-Energy Nexus 4, 95–102. https://doi.org/10.1016/j.wen.2021.06.001.
Santos, B.L.C., Parpot, P., Soares, O.S.G.P., Pereira, M.F.R., Rombi, E., Fonseca, A.M., Correia Neves, I., 2020. Fenton-type bimetallic catalysts for degradation of dyes in aqueous solutions. Catalysts 11, 32. https://doi.org/10.3390/catal11010032.
Satopaa, V., Albrecht, J., Irwin, D., Raghavan, B., 2011. Finding a "Kneedle" in a Haystack: Detecting Knee Points in System Behavior, in: 2011 31st International Conference on Distributed Computing Systems Workshops. IEEE, pp. 166–171. https://doi.org/10.1109/ICDCSW.2011.20.
Shannon, R.D., 1976. Revised effective ionic radii and systematic studies of interatomic distances in halides and chalcogenides. Acta Crystallographica Section A 32, 751–767. https://doi.org/10.1107/S0567739476001551.
Sievers, M., 2011. Advanced Oxidation Processes, in: Treatise on Water Science. Elsevier, pp. 377–408. https://doi.org/10.1016/B978-0-444-53199-5.00093-2.
Silva, M.M., Reboredo, F.H., Lidon, F.C., 2022. Food colour additives: a synoptical overview on their chemical properties, applications in food products, and health side effects. Foods 11, 379. https://doi.org/10.3390/foods11030379.
Unal Yesiller, S., Eroğlu, A.E., Shahwan, T., 2013. Removal of aqueous rare earth elements (REEs) using nano-iron based materials. J. Ind. Eng. Chem. 19, 898–907. https://doi.org/10.1016/j.jiec.2012.11.005.
Villalba, J.C., Constantino, V.R.L., Anaissi, F.J., 2010. Iron oxyhydroxide nanostructured in montmorillonite clays: preparation and characterization. J. Colloid Interface Sci. 349, 49–55. https://doi.org/10.1016/j.jcis.2010.04.057.
Wang, W., Zhang, W., Chen, H., Zhang, S., Li, J., 2015. Synergistic effect of synthetic zeolites on flame-retardant wood-flour/polypropylene composites. Constr. Build. Mater. 79, 337–344. https://doi.org/10.1016/j.conbuildmat.2015.01.038.
Xu, R., Pang, W., Yu, J., Huo, Q., Chen, J., 2007. Chemistry of Zeolites and Related Porous Materials, Chemistry of Zeolites and Related Porous Materials: Synthesis and Structure. Wiley. https://doi.org/10.1002/9780470822371.
Yang, W., Fidelis, T.T., Sun, W.-H., 2020. Machine learning in catalysis, from proposal to practicing. ACS Omega 5, 83–88. https://doi.org/10.1021/acsomega.9b03673.
Yang, F., Kubota, F., Baba, Y., Kamiya, N., Goto, M., 2013. Selective extraction and recovery of rare earth metals from phosphor powders in waste fluorescent lamps using an ionic liquid system. J. Hazard. Mater. 254–255, 79–88. https://doi.org/10.1016/j.jhazmat.2013.03.026.
Zhao, F., Repo, E., Meng, Y., Wang, X., Yin, D., Sillanpää, M., 2016. An EDTA-β-cyclodextrin material for the adsorption of rare earth elements and its application in preconcentration of rare earth elements in seawater. J. Colloid Interface Sci. 465, 215–224. https://doi.org/10.1016/j.jcis.2015.11.069.
Zheng, B., Fan, J., Chen, B., Qin, X., Wang, J., Wang, F., Deng, R., Liu, X., 2022. Rare-Earth doping in nanostructured inorganic materials. Chem. Rev. 122, 5519–5603. https://doi.org/10.1021/acs.chemrev.1c00644.